

# NJC

Accepted Manuscript



This is an *Accepted Manuscript*, which has been through the Royal Society of Chemistry peer review process and has been accepted for publication.

*Accepted Manuscripts* are published online shortly after acceptance, before technical editing, formatting and proof reading. Using this free service, authors can make their results available to the community, in citable form, before we publish the edited article. We will replace this *Accepted Manuscript* with the edited and formatted *Advance Article* as soon as it is available.

You can find more information about *Accepted Manuscripts* in the [Information for Authors](#).

Please note that technical editing may introduce minor changes to the text and/or graphics, which may alter content. The journal's standard [Terms & Conditions](#) and the [Ethical guidelines](#) still apply. In no event shall the Royal Society of Chemistry be held responsible for any errors or omissions in this *Accepted Manuscript* or any consequences arising from the use of any information it contains.



[www.rsc.org/njc](http://www.rsc.org/njc)

## Theoretical investigation on the effects of N-substitution on the photophysical properties of two series of iridium(III) complexes

Xiaohong Shang,<sup>\*a</sup> Deming Han,<sup>b</sup> Qing Zhan,<sup>c</sup> Defeng Zhou,<sup>a</sup> and Gang Zhang<sup>d</sup>

<sup>a</sup> College of Chemistry and Life Science, Changchun University of Technology, Changchun 130012, P. R. China

E-mail: shangxiaohong58@aliyun.com

<sup>b</sup> School of Life Science and Technology, Changchun University of Science and Technology, Changchun 130022, P. R. China

<sup>c</sup> Jilin Provincial Institute of Education, Changchun 130022, P.R. China

<sup>d</sup> State Key Laboratory of Theoretical and Computational Chemistry, Institute of Theoretical Chemistry, Jilin University, Changchun 130023, P. R. China

Based on the complexes  $[\text{Ir}(\text{dfb-pz})_2(\text{tfmty})]$  (1) and  $[\text{Ir}(\text{tfmfb-pz})_2(\text{tfmty})]$  (2) [dfb-pz = 2,4-difluorobenzyl-*N*-pyrazole; tfmty = 2-(5-trifluoromethyl-[1,2,4]triazol-3-yl)-pyridine; tfmfb-pz = 2-tri-fluoromethyl-5-fluorobenzyl-*N*-pyrazole], two series of Ir(III) complexes are designed by substituting “CH” groups with the N atom at -a, -b, -c, and -d positions on the pyridine moiety in N<sup>^</sup>N ligands. The electronic structure, absorption and emission spectra as well as phosphorescence efficiency of all these Ir(III) complexes were investigated by using density functional theory (DFT) and time-dependent DFT (TDDFT) methods. The calculated results show that the assumed complexes 1a and 2a may possess a higher photoluminescent quantum efficiency than other complexes and are the potential candidates as the efficient blue-emitting material. The study shows that the N substitution can tune the emitting color of 1 and 2 and enhance the photoluminescence quantum efficiency.

## Introduction

Phosphorescent transition-metal complexes have attracted great attention in the development of highly efficient organic light-emitting devices (OLEDs).<sup>1-5</sup> Due to the heavy-atom induced spin-orbit coupling (SOC) effect, which can partially remove the spin-forbidden nature of the  $T_1 \rightarrow S_0$  radiative relaxation, the electrophosphorescence can make use of both singlet and triplet excitons and achieve a theoretical level of unity for the internal quantum efficiency, rather than the 25% inherent upper limit imposed by the formation of singlet excitons for the respective fluorescent materials.<sup>6-8</sup> Thus, considerable efforts have been devoted to the second- and third-row transition metal complexes to develop highly efficient phosphors that can emit the three primary colors, which are the essential components for full-color displays.

Cyclometalated iridium(III) complexes are known to be the very promising candidates as OLEDs phosphors,<sup>7,9</sup> which can display phosphorescent emission spanning the whole visible spectrum.<sup>10-12</sup> Highly efficient red and green phosphorescent iridium(III) complexes in OLEDs have been realized during the past years, but it is still challenging to develop a stable and efficient device in the blue spectral range.<sup>13</sup> Such a color is needed for white light generation, which involves a wide range of applications in full-color displays and solid state lighting. Thus, many efforts have been devoted toward the design, synthesis, and photophysical investigation on the new blue-emitting phosphorescent iridium(III) complexes.

Generally, useful approaches of the systematic tuning for Ir(III)-based blue emitters are less obvious and have been summarized by Thompson and coworkers:<sup>14-16</sup> (a) use of electron-withdrawing substituents at the cyclometalating ring, for instance, fluoride. If the fluoride was attached on the main ligand, it can effect the highest occupied molecular orbital (HOMO) level (both from the metal and main ligand orbitals), whereas only slightly affecting the lowest unoccupied molecular orbital (LUMO) level (from the auxiliary ligand); conversely, if the fluoride was attached on the auxiliary ligand, it can effect the LUMO level more, whereas HOMO level slightly; (b) use of ancillary ligands to tune the HOMO and

LUMO energies of Ir complexes. The approach based on the electron perturbation of the HOMO–LUMO energy gap, the emission coming from the metal and the ligands fragments. (c) replacement of the heterocyclic fragment of the ligands, like phenylpyridine, with moieties bearing higher lying LUMO than for the pyridyl ring, this can raise the energy of both the metal to ligand charge transfer (MLCT) and the ligand centered (LC) transitions. The most commonly used electron withdrawing group is fluoride and the representative blue phosphors are a class of iridium(III) complexes possessing at least one cyclometalated 4,6-difluorophenyl pyridine {(dfppy)H} ligand, known as FIrpic,<sup>16</sup> FIr6,<sup>17</sup> FIrtaz,<sup>18</sup> and others. Besides, since the photophysical properties and related applications of the cyclometalated iridium(III) complexes are strongly dependent on the characteristics of their ground and lowest excited states, it has become desirable to better understand the interactions between these states and thus determine how to systematically alter the photophysical properties by appropriate ligand or complex design.

For the realization of full-color displays, Chi *et al.* have reported a class of potential blue-emitting phosphors of Ir(III) complexes [(Ir(df<sub>2</sub>b-pz)<sub>2</sub>(tfmty<sub>2</sub>p)) (1) and [Ir(tfmfb-pz)<sub>2</sub>(tfmty<sub>2</sub>p)] (2) (Fig. 1) [df<sub>2</sub>b-pz = 2,4-difluorobenzyl-*N*-pyrazole; tfmty<sub>2</sub>p = 2-(5-trifluoromethyl-[1,2,4]triazol-3-yl)-pyridine; tfmfb-pz = 2-tri-fluoromethyl-5-fluorobenzyl-*N*-pyrazole] with nonconjugated bidentate ligand.<sup>19</sup> Herein, two series of derivatives by a systematic substitution of the “CH” group by the electron-withdrawing nitrogen (N) atom at -a, -b, -c, and -d positions on the pyridine moiety of tfmty<sub>2</sub>p (N<sup>^</sup>N) ligands in 1 and 2, respectively, (Fig. 1) have been designed in order to investigate the influence of substitution on photophysical and spectra properties of these Ir(III) complexes. It is anticipated that this study can be of great benefit for designing novel and highly efficient blue-emitting Ir(III) complexes.

## Computational methods

The ground state and the lowest lying triplet excited state geometries were carried out using the density functional theory (DFT)<sup>20</sup> with hybrid Hartree-Fock/density

functional model (PBE0) based on the Perdew-Burke-Erzenrhof (PBE).<sup>21</sup> Restricted and unrestricted<sup>22</sup> formalisms were adopted in the singlet and triplet geometry optimization, respectively. All geometrical structures were fully optimized without any symmetry constraints. Vibrational frequencies were also calculated at the same theoretical level, which confirms that each configuration was a minimum on the potential energy surface. In order to choose the suitable calculation method, Becke's three parameter hybrid method<sup>23</sup> combined with the Lee-Yang-Parr correlation functional<sup>24</sup> (denoted as B3LYP) is also applied. The basis set effect has been tested using different combinations of basis sets for metal and rest of the other (C, H, N, F) atoms. The quasi-relativistic pseudopotentials of Ir atoms proposed by Hay and Wadt with 17 valence electrons were employed, and a "double- $\zeta$ " quality basis set LANL2DZ was adopted as the basis set.<sup>25</sup> For other atoms, 6-31G(d), 6-31+G(d), and 6-311+G(d) basis sets were employed. On the basis of the optimized ground- and lowest excited-state equilibrium geometries, the time-dependent density functional theory (TDDFT)<sup>26</sup> approach associated with the polarized continuum model (PCM)<sup>27</sup> in dichloromethane (CH<sub>2</sub>Cl<sub>2</sub>) media was applied to investigate the absorption and emission spectral properties from the experimental results by Chi *et al.*<sup>19</sup> The S<sub>1</sub>-T<sub>1</sub> energy gap ( $\Delta E_{S_1-T_1}$ ) was calculated by considering the fixed triplet molecular geometry. All calculations were performed with the B.01 revision of the Gaussian 09 program package,<sup>28</sup> the GaussSum 2.5 program<sup>29</sup> being used for the UV/Vis absorption spectral analysis with the full width at half maximum (FWHM) value of 3000 cm<sup>-1</sup> based on the data obtained via TDDFT calculations.

## Results and discussion

### Computational Methods and Basis Sets

In order to verify the reliability of the calculation method, the structure parameters of complexes **1** and **2** (Fig. 1) studied here, has been computed with the PBE0 and B3LYP methods using the different basis sets and compared with the experimental results<sup>[19]</sup> (X-ray crystal structure data) (see Table S1 (Supporting Information) for

details).

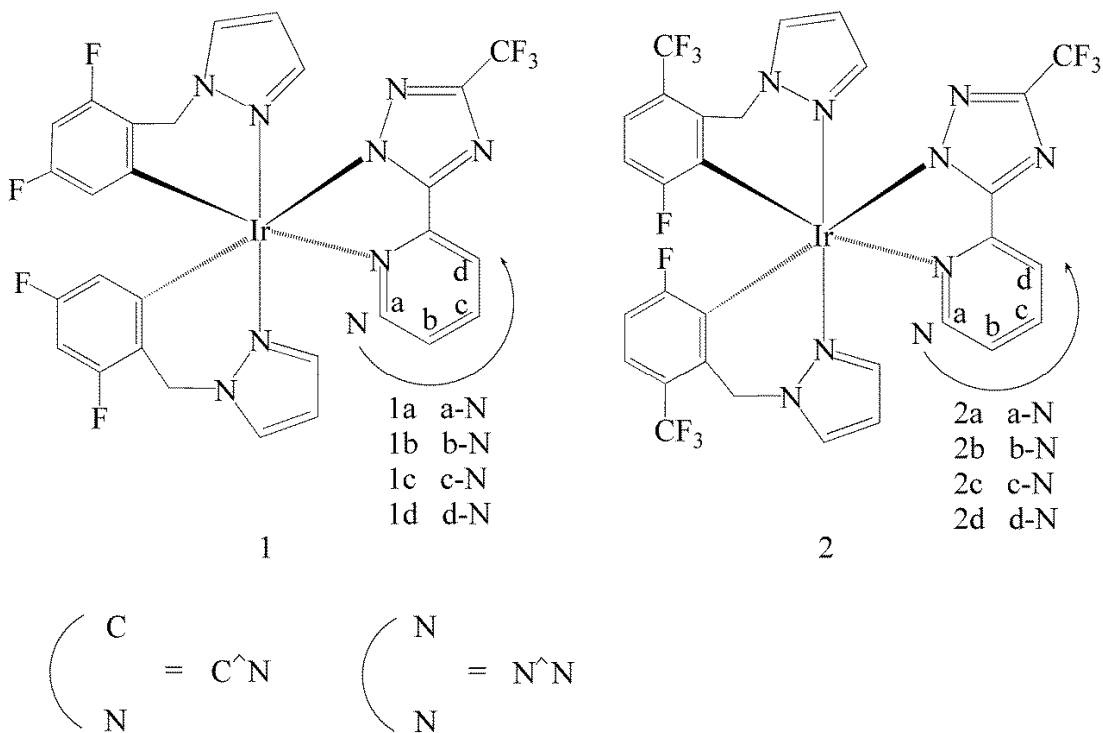


**Fig. 1** Schematic structures of the investigated complexes [x-N ( $x = a, b, c, d$ ) represents the “CH” group at the  $x$ -position substituted by the N atom].

The optimized structures of **1** and **2** in the ground state at PBE0 level is shown in Fig. 2 along with the numbering of some key atoms.

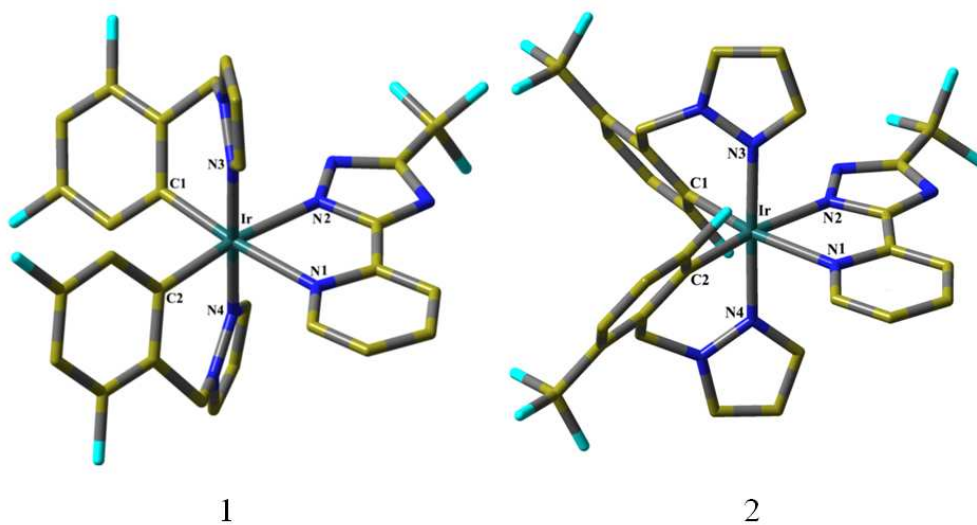


**Fig. 2** Optimized structure of **1** and **2** in the ground state.

Fig. S1 (Supporting Information) showed the variations of the calculated bond lengths compared with the experimental results for complexes **1** and **2**. A good agreement with experimental data was obtained for DFT/PBE0 method with 6-31G(d), 6-31+G(d), and 6-311+G(d) basis sets, even though it overestimates Ir-N1 bond lengths with the variation more than 0.039 Å, while a disagreement was found for B3LYP method, especially the bond lengths of Ir-N1 with the deviation more than 0.091 Å. Hence, PBE0 is a better method to give theoretical insights into this kind of compounds. Because the basis set does not have much effect on the structural parameters, the calculated data from the basis set of 6-31G(d) are good enough to predict the structures and properties of these complexes.

### Molecular geometries in ground and lowest triplet states

The schematic structures of the investigated complexes are depicted in Fig. 1 (the cyclometalated and ancillary ligands are denoted as C<sup>N</sup> and N<sup>N</sup>, respectively). The fully optimized ground state structures of **1** and **2** are presented in Fig. 2 along with the numbering of some key atoms. The main optimized geometry parameters for these complexes in ground state (S<sub>0</sub>) and lowest lying triplet excited state (T<sub>1</sub>) are summarized in Table 1.

**Table 1** Main optimized geometry parameters of the investigated complexes in the ground and the lowest lying triplet states

	1		1a		1b		1c		1d	
	S <sub>0</sub>	T <sub>1</sub>								
Bond Length/Å										
Ir-N1	2.219	2.181	2.208	2.162	2.212	2.183	2.209	2.171	2.209	2.180
Ir-N2	2.136	2.100	2.127	2.038	2.134	2.037	2.122	2.106	2.133	2.066
Ir-N3	2.046	2.045	2.048	2.009	2.046	2.033	2.047	2.045	2.047	2.042
Ir-N4	2.036	2.040	2.041	2.048	2.042	2.048	2.041	2.041	2.039	2.044
Ir-C1	2.022	2.030	2.019	2.044	2.021	2.032	2.020	2.031	2.022	2.031

Ir-C2	2.031	2.034	2.030	2.042	2.030	2.049	2.030	2.031	2.032	2.041
Bond Angle/deg										
N1-Ir-N2	75.8	77.2	75.6	77.5	75.5	77.9	75.8	77.0	75.3	77.4
C1-Ir-N3	88.7	89.0	88.8	89.7	88.7	89.1	88.6	89.0	88.6	89.0
C2-Ir-N3	92.1	89.5	89.6	86.5	89.8	87.8	89.9	89.4	89.9	88.9
	2		2a		2b		2c		2d	
	S <sub>0</sub>	T <sub>1</sub>								
Bond Length/Å										
Ir-N1	2.207	2.164	2.180	2.101	2.201	2.159	2.200	2.150	2.199	2.150
Ir-N2	2.100	2.072	2.087	2.065	2.094	2.038	2.087	2.074	2.094	2.055
Ir-N3	2.044	2.043	2.043	2.037	2.045	2.039	2.045	2.043	2.045	2.042
Ir-N4	2.044	2.045	2.049	2.036	2.045	2.041	2.046	2.045	2.045	2.044
Ir-C1	2.039	2.048	2.040	2.057	2.037	2.053	2.038	2.050	2.038	2.051
Ir-C2	2.056	2.060	2.051	2.054	2.055	2.067	2.056	2.058	2.057	2.064
Bond Angle/deg										
N1-Ir-N2	76.4	77.7	76.6	77.9	76.2	78.3	76.5	77.6	76.1	77.8
C1-Ir-N3	86.0	86.4	85.8	86.5	86.0	86.8	85.9	86.5	85.9	86.4
C2-Ir-N3	94.6	86.1	86.4	86.3	86.4	85.7	86.5	86.0	86.5	86.1

It can be seen that all complexes studied here adopt a pseudo-octahedral coordination geometry, with *cis*-N1,N2 and *trans*-N3,N4 chelate disposition.

The results show that the introduction of the electron-withdrawing N atom at -a, -b, -c, and -d positions on the pyridine moiety of the N<sup>^</sup>N ligand in complexes 1 and 2 cause obvious changes in the Ir–N1 and Ir–N2 (Table 1). It is noted that the Ir–C (Ir–C1 and Ir–C2) and Ir–N (Ir–N3 and Ir–N4) bond lengths show negligible changes (within ~0.006 Å), indicating that the introduction of the N substituent on the pyridine moiety of N<sup>^</sup>N ligands in 1 and 2 causes a minor effect on the geometric structures for C<sup>^</sup>N ligands. For 1a–1d (1 represents complex 1, while a, b, c and d indicates N substitution at -a, -b, -c, and -d positions. 1a–1d indicates 1a, 1b, 1c, and 1d. A similar definition was applied to complex 2) and 2a–2d, the bond lengths of Ir–N1 and Ir–N2

are significantly shortened compared to those of unsubstituted complexes 1 and 2 (Table 1), leading to the strengthened coordination interaction between Ir(III) center and N<sup>^</sup>N ligands, which may also increase the probability of charge transfer from metal to N<sup>^</sup>N ligands. More interesting, the degree that the bond lengths shortened is very sensitive to the N substituted positions. For 1a, 1c, 2a, and 2c in which the N substitution is at the -a position and -c position, the changes are the largest.

In order to demonstrate the changes of geometry parameters upon excited, the geometry parameters of all complexes in the triplet excited states were also calculated. The changes of the selected Ir(III)-related bond lengths from ground to excited state are shown in Fig. S2 (Supporting Information). No obvious variations for the bond distances of Ir–N3, Ir–N4, Ir–C1, and Ir–C2 are found from S<sub>0</sub> to T<sub>1</sub> states (with the nearly negligible difference within 0.02 Å). In addition, Ir–N1 and Ir–N2 bond lengths are shortened significantly on the excited state compared with those in S<sub>0</sub> states especially in 1a and 2a (more than 0.022 Å), resulting in the strengthened interaction between metal and N<sup>^</sup>N ligands in T<sub>1</sub> states, which might consequently cause the decrease of metal-centered (MC) nonradiative emission and the enhancement of radiative deactivation compared with other complexes. Besides, complexes 1a–1d and 2a–2d have the similar changes of geometry parameters in comparison to 1 and 2, respectively.

### Frontier molecular orbitals analysis

The spectral properties are closely related to the characters of the frontier molecular orbitals (FMOs). Tables S2–S11 (Supporting Information) have provided the FMOs compositions for studied complexes. The highest occupied molecular orbital (HOMO) and lowest unoccupied molecular orbital (LUMO) distribution, energy levels, and HOMO-LUMO energy gaps are plotted in Fig. 3.

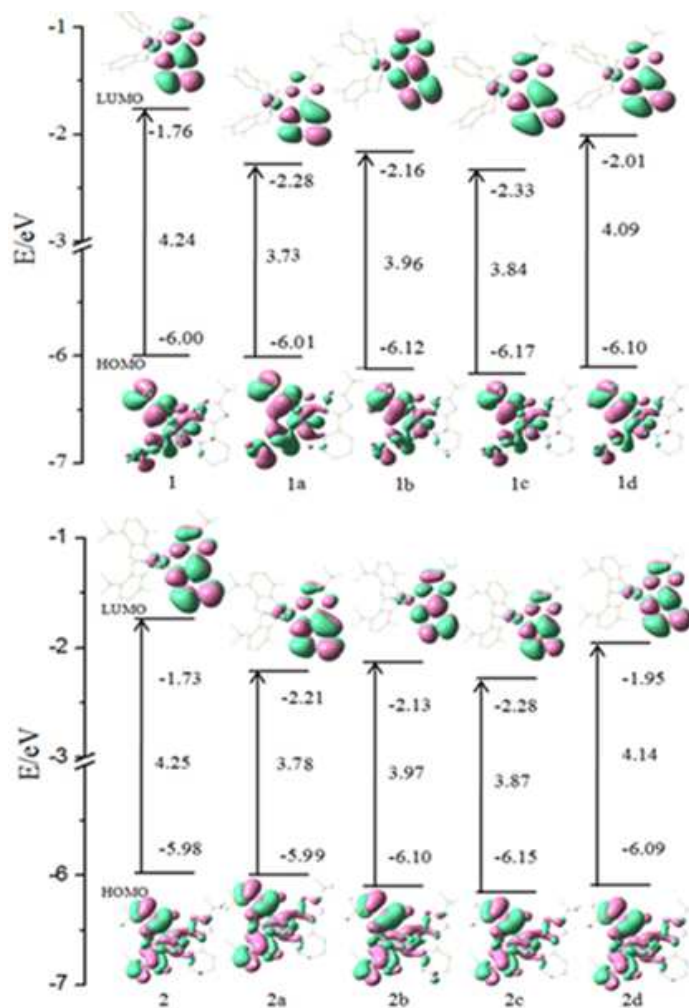


**Fig. 3** Energy level, energy gaps (in eV), and orbital composition distribution of HOMO and LUMO for the studied complexes.

For complex 1, the HOMO is composed of 36% Ir d-orbital, antibonding combination with 62%  $\pi$ -orbital of C<sup>^</sup>N moiety with negligible composition from N<sup>^</sup>N moiety. Complex 2 has an orbital composition very similar to that of 1, and slightly enhances the contribution from metal d-orbital (shown in Table S7). For 1 and 2, although the energies of HOMO and LUMO are different due to the different C<sup>^</sup>N ligands, i.e., HOMO lying at -6.00 eV and LUMO -1.76 eV in 1, HOMO lying at -5.98 eV and LUMO -1.73 eV in 2, the energy gaps are nearly the same, i.e., 4.24 eV for 1 and 4.25 eV for 2. This indicates that the change of C<sup>^</sup>N ligands from -F substitution in 1 to the stronger electron-withdrawing group of -CF<sub>3</sub> in 2 alters the

energy levels, but not the energy gap. The electron density of HOMO of 1a-1d and 2a-2d are predominantly localized on the Ir(III) center (35-39%) and the  $\pi(\text{C}^{\wedge}\text{N})$  (56-63%), while LUMO has the predominant  $\pi^*(\text{C}^{\wedge}\text{N})$  characters. The electron densities of the HOMO and LUMO distributions are hardly influenced by the N substitution on the pyridine moiety of  $\text{C}^{\wedge}\text{N}$  ligands in complexes 1 and 2.

The introduction of the N substituent at different positions of the pyridine moiety in  $\text{N}^{\wedge}\text{N}$  ligands has a significant effect on FMOs energy levels as shown in Fig. 3. For 1a-1d and 2a-2d, the N substitution stabilizes the HOMO and LUMO energy levels because the N substituent withdraws electrons from the complexes. The decreasing tendency of the LUMO energy level is more significant than that of HOMO, which results in a decrease of the HOMO-LUMO energy gap in comparison with those of 1 and 2. As shown in Fig. 3, in comparison to 1 and 2, complexes 1a and 2a have the significantly lower LUMO energy levels, the slightly reduced HOMO levels. Besides, 1a and 2a have the smallest HOMO-LUMO energy gaps among these complexes. It is noted that the N substitution at the -c position (1c and 2c) not only more dramatically affects the LUMO energy level than the other substituent positions, but also results in the obvious decrease of the HOMO energy level. In addition, the energy levels of LUMO and HOMO for 1d and 2d also show a slight reduction in comparison to 1 and 2. The N substituent at different positions of the pyridine moiety in  $\text{N}^{\wedge}\text{N}$  ligands has a significant effect on changing the HOMO-LUMO gap, because it can change the energy of one orbital, such as LUMO, resulting in the blue shift for the absorption and phosphorescence wavelengths.

#### **Absorption spectra in $\text{CH}_2\text{Cl}_2$ media**

TDDFT/PBE0/LANL2DZ+6-31G(d) method with PCM in  $\text{CH}_2\text{Cl}_2$  media has been used to study the nature and the energy of absorption spectra of these complexes on the basis of the optimized  $S_0$  geometries. Simulated absorption spectra of these Ir complexes are sketched in Fig. 4.

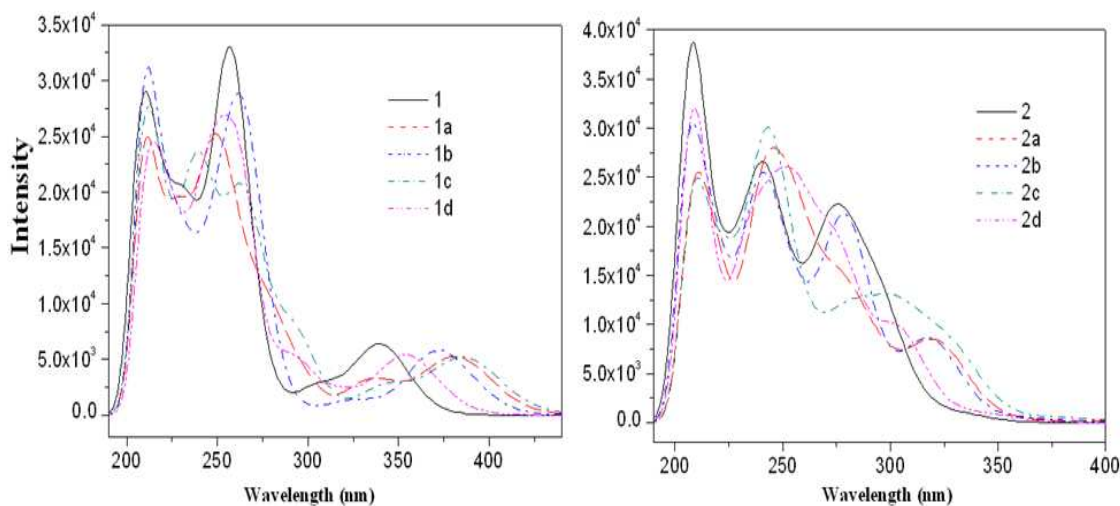


**Fig. 4** Simulated absorption spectra of 1-1d and 2-2d, respectively, in  $\text{CH}_2\text{Cl}_2$  media.

The transition energies, oscillator strengths and configurations for the relevant lowest singlet excited states and the lowest triplet state in each complex are listed in Table S12 accompanying with the experimental results.

The experimental absorption spectra for complexes 1 and 2 show the intense features below 300 nm and less intense features in the range 300-400 nm.<sup>19</sup> It can be seen that the lowest energy absorption wavelengths calculated follow the order: 1(357 nm) > 1d(363 nm) > 1b(383 nm) > 1a(395 nm) > 1c(399 nm) and 2(360 nm) > 2d(380 nm) > 2b(402 nm) > 2a(413 nm) > 2c(418 nm), which is not closely related to the variation trend of HOMO–LUMO energy gaps because HOMO→LUMO transition configurations are not predominantly contributed by  $S_0 \rightarrow S_1$  transitions for all cases because the  $S_1$  state for 1c and 2c comes from the HOMO→LUMO/LUMO+1 transition. As a result of the negligible intensity for 1c (0.000) / 2c (0.001), the  $S_0 \rightarrow S_1$  transition is probably forbidden and would be practically absent in the absorption spectra. The calculated lowest-lying singlet absorptions at 357 and 360 nm for 1 and 2 are in good agreement with the experimental values at 368 and 370 nm,<sup>19</sup> respectively. In addition, in the experimental spectra, one maximal peaks located at around 261 and 284 nm are shown for 1 and 2 respectively, while the TDDFT calculations at 256 and 292 nm (Table S12) also agree well with the experimental data. The transition

configuration of HOMO-3→LUMO+1 contributes to the 256 nm absorption peaks with the largest oscillator strength for 1 described as the  $[d(\text{Ir})+\pi(\text{C}^{\wedge}\text{N}+\text{N}^{\wedge}\text{N})\rightarrow\pi^*(\text{N}^{\wedge}\text{N})]$  transition, while the HOMO→LUMO+4 excitations for 246 nm (experimental values at 261 nm) absorption of 2 with the mixed transition characters of MLCT(metal to ligand charge transfer)/LLCT(ligand to ligand charge transfer)/ILCT (intraligand charge transfer).

The calculated lowest-lying absorption bands for 1a-1d exhibit a red-shift with 395, 383, 399 and 363 nm compared to 357 nm for 1. Similar, it also exhibits a red-shift with 413, 402, 418 and 380 nm for 2a-2d compared to 360 nm for 2 (Table S12). The  $S_1$  states are predominantly contributed to by the HOMO→LUMO transition with more than 90% in composition except that the  $S_1$  states of 1c and 2c are mainly contributed to by HOMO→LUMO (56%) / HOMO→LUMO+1 (38%) and HOMO→LUMO (53%) / HOMO→LUMO+1 (38%), respectively. From the analysis on FMOs, it is reasonable to assign the lowest-lying absorptions to mainly  $[d(\text{Ir})+\pi(\text{C}^{\wedge}\text{N})\rightarrow\pi^*(\text{N}^{\wedge}\text{N})]$  with MLCT and LLCT characters. For 1a-1d, the transitions with the largest oscillator strengths are located at 248, 266, 270 and 263 nm, for 2a-2d, the transitions with the largest oscillator strengths are located at 241, 280, 242 and 245 nm, respectively, and have the transition characters of MLCT/LLCT/ILCT. In regard to 1a-1d and 2a-2d, the transition compositions are located at around 50% contribution to the largest oscillator strength absorption.

### Phosphorescence in $\text{CH}_2\text{Cl}_2$ media

TDDFT method was used to calculate the phosphorescent spectra in  $\text{CH}_2\text{Cl}_2$  media on the basis of the lowest triplet state geometries. To obtain reliable results, four DFT functionals (M062X, M052X, B3LYP, and PBE0) were examined here. The results show that the calculated triplet excited energies of the complexes 1 and 2 with the M062X functional are more close to the experimental values<sup>19</sup> (Table S13). Therefore, we have employed the M062X functional for further emission spectra calculations. The calculated emission energies, transition nature, and the available experimental values are listed in Table 2.

**Table 2** Calculated phosphorescent emission of the studied complex in CH<sub>2</sub>Cl<sub>2</sub> media at the TDDFT/M062X level, together with the experimental values

complexes	$\lambda(\text{nm})/E(\text{eV})$	Configuration	Character	Exptl. <sup>a</sup>
1	456/ 2.71	L→H(69%)	$\pi^*(\text{N}^{\wedge}\text{N})\rightarrow\text{d}(\text{Ir})+\pi(\text{C}^{\wedge}\text{N})$ (MLCT/LLCT)	460
1a	412/ 3.00	L→H(57%)	$\pi^*(\text{N}^{\wedge}\text{N})\rightarrow\text{d}(\text{Ir})+\pi(\text{C}^{\wedge}\text{N})$ (MLCT/LLCT)	
1b	433/ 2.85	L→H(45%)	$\pi^*(\text{N}^{\wedge}\text{N})\rightarrow\text{d}(\text{Ir})+\pi(\text{C}^{\wedge}\text{N})$ (MLCT/LLCT)	
1c	493/ 2.51	L→H(44%)	$\pi^*(\text{N}^{\wedge}\text{N})\rightarrow\text{d}(\text{Ir})+\pi(\text{C}^{\wedge}\text{N})$ (MLCT/LLCT)	
		L→H-2(31%)	$\pi^*(\text{N}^{\wedge}\text{N})\rightarrow\pi(\text{C}^{\wedge}\text{N})$ (LLCT)	
1d	444/ 2.78	L→H(51%)	$\pi^*(\text{N}^{\wedge}\text{N})\rightarrow\text{d}(\text{Ir})+\pi(\text{C}^{\wedge}\text{N})$ (MLCT/LLCT)	
2	457/ 2.70	L→H(65%)	$\pi^*(\text{N}^{\wedge}\text{N})\rightarrow\text{d}(\text{Ir})+\pi(\text{C}^{\wedge}\text{N}+\text{N}^{\wedge}\text{N})$ (MLCT/LLCT/ILCT)	457
2a	427/ 2.90	L→H(72%)	$\pi^*(\text{N}^{\wedge}\text{N})\rightarrow\text{d}(\text{Ir})+\pi(\text{C}^{\wedge}\text{N})$ (MLCT/LLCT)	
2b	434/ 2.85	L→H(77%)	$\pi^*(\text{N}^{\wedge}\text{N})\rightarrow\text{d}(\text{Ir})+\pi(\text{C}^{\wedge}\text{N})$ (MLCT/LLCT)	
2c	493/ 2.51	L→H(67%)	$\pi^*(\text{N}^{\wedge}\text{N})\rightarrow\text{d}(\text{Ir})+\pi(\text{C}^{\wedge}\text{N})$ (MLCT/LLCT)	
2d	449/ 2.76	L→H(74%)	$\pi^*(\text{N}^{\wedge}\text{N})\rightarrow\text{d}(\text{Ir})+\pi(\text{C}^{\wedge}\text{N})$ (MLCT/LLCT)	

<sup>a</sup> Reference 19

To conveniently discuss the transition property of emission, the partial compositions of FMOs related to emission are listed in Table S14. In regard to 1, the excitation of HOMO→LUMO is responsible for the emission at 456 nm (see Table 2). Table S14 shows that HOMO has 35% d(Ir) and 63%  $\pi(\text{C}^{\wedge}\text{N})$ , while LUMO is  $\pi^*(\text{N}^{\wedge}\text{N})$  type orbital. Thus the emission at 456 nm originates from [ $\pi^*(\text{N}^{\wedge}\text{N})\rightarrow\text{d}(\text{Ir})+\pi(\text{C}^{\wedge}\text{N})$ ] excited states with MLCT / LLCT characters. For 1a-1d with N substitution in N<sup>^</sup>N ligands, one transition of LUMO–HOMO are responsible for the emission, which is blue-shifted evidently compared with that of 1 with the exception of 1c. For 1c with the N atom incorporated, the excitations of LUMO→HOMO (44%) and LUMO→HOMO–2 (31%) mixed transitions assigned to [ $\pi^*(\text{N}^{\wedge}\text{N})\rightarrow\text{d}(\text{Ir})+\pi(\text{C}^{\wedge}\text{N})$ ] and  $\pi^*(\text{N}^{\wedge}\text{N})\rightarrow\pi(\text{C}^{\wedge}\text{N})$  with the mixed characters of MLCT and LLCT are responsible for the emission at 493 nm. Table 2 and Table S14 show that the nature of the phosphorescence for 2–2d is similar to that of 1–1d, they originate

from MLCT/LLCT and MLCT/LLCT/ILCT characters, respectively.

From the above calculation results, it can be seen that the N atom substitution change the transition character of the emission and the emission color. Complexes 1a, 1b, 1d, 2a, 2b and 2d could be blue-emitters, while 1c and 2c could be a red-emitter. These results will be very important for designing excellent phosphorescent heavy-metal complexes with the tunable optical and electronic properties.

### Efficiency comparison

Generally, there are three processes to govern the phosphorescence quantum yields ( $\Phi$ ): (a) singlet–triplet intersystem crossing (ISC); (b) radiative decay from a triplet state to the singlet ground state; (c) nonradiative decay from an excited state to the ground state. If one emitter has fast processes (a) and (b), and slow process (c), it will be a strong emitter.<sup>30</sup> The  $\Phi$  can be expressed as equation:

$$\Phi = k_r \tau_{em} = \frac{k_r}{k_r + k_{nr}} \quad (1)$$

where  $\tau_{em}$  is the emission decay time,  $\Phi$  can be affected by the competition between  $k_r$  (radiative rate constants) and  $k_{nr}$  (non-radiative rate constants). Therefore, to increase the quantum yield, a large  $k_r$  and a small  $k_{nr}$  are required. The rate constants for phosphorescence, expressed as:

$$k_r \approx \gamma \frac{\langle \Psi_{S_1} | H_{S_0} | \Psi_{T_1} \rangle^2 \mu_{S_1}^2}{(\Delta E_{S_1-T_1})^2}, \quad \gamma = \frac{16\pi^3 10^6 n^3 E_{em}^3}{3h\epsilon_0} \quad (2)$$

where  $\mu_{S_1}$  is the transition electric dipole moment in  $S_0 \rightarrow S_1$  transition;  $E_{em}$  represents the emission energy in  $\text{cm}^{-1}$  and  $n$ ,  $h$ , and  $\epsilon_0$  are the refractive index, Planck's constant, and the permittivity in vacuum, respectively. According to the equation, the  $\Delta E_{S_1-T_1}$  was the  $S_1$ - $T_1$  energy gap. Theoretically,  $k_r$  is related to the mixing between  $S_1$  and  $T_1$ , which is proportional to spin-orbit coupling (SOC) and inversely proportional to the energy difference between  $S_1$  and  $T_1$  states. The presence of a heavy atom, such

as iridium, is anticipated to increase SOC effects and thus intersystem crossing (ISC), on the condition that its orbitals make a significant contribution to the excited states involved. The SOC effects can be elucidated by the metal contribution (MLCT %) in the  $T_1$  state.<sup>31</sup> The direct involvement of the Ir(III) d orbital can enhance the SOC effects in the  $T_1 \rightarrow S_0$  transition, which would result in a drastic decrease of the radiative lifetime and reduce the possibility of nonradiative process.<sup>32,33</sup> Thus, a large MLCT contribution is then beneficial to increase the  $k_r$ . From Table 3, we noted that the MLCT% is found to be affected by the different positions of N atom for these complexes.

**Table 3** Computed metal-based charge transfer character  $^3\text{MLCT}$  (%), singlet-triplet splitting energy  $\Delta E_{S_1-T_1}$  (eV), transition dipole moment in the  $S_0 \rightarrow S_1$  transition  $\mu_{S_1}$  (Debye) for complexes 1a-1d and 2a-2d, along with the measured quantum yield  $\Phi$ , radiative rate constant  $k_r$  ( $\times 10^6 \text{ s}^{-1}$ ) and nonradiative rate constant  $k_{nr}$  ( $\times 10^6 \text{ s}^{-1}$ ) for complexes 1 and 2

complex	$\Phi^a$	$k_r^a$	$k_{nr}^a$	$^3\text{MLCT}$	$\Delta E_{S_1-T_1}$	$\mu_{S_1}$
1	0.04	0.6	14	23.46	0.8965	0.39
1a				18.24	0.3097	0.47
1b				15.30	0.5011	0.35
1c				14.08	0.6588	0.37
1d				16.32	0.6585	0.44
2	0.10	1.0	9	23.40	0.7174	0.22
2a				24.48	0.2218	0.40
2b				27.72	0.2821	0.32
2c				23.45	0.4757	0.17
2d				25.90	0.4903	0.37

<sup>a</sup> Reference 19

The introduction of N substituent on the pyridine moiety in N<sup>^</sup>N ligands decreases MLCT% for 1a-1d, whereas 2a-2d has the opposite change trend. The contribution of MLCT is calculated to be 23.46% and 23.40% for 1 and 2 and an approximately equal MLCT contribution is observed, while the experimental observed  $\Phi$  of 2 (10%) is two times larger than that of 1 (4%), therefore it was concluded that the MLCT contribution does not contribute significantly to the quantum yields. In addition, the S<sub>1</sub>-T<sub>1</sub> energy gap ( $\Delta E_{S_1-T_1}$ ) is the factor that affects the SOC effects.<sup>22</sup> The S<sub>1</sub>→T<sub>1</sub> ISC induced by SOC interactions plays an important role in the phosphorescent process. Through equation (2), we can see that both a decrease of  $\Delta E_{S_1-T_1}$  and a larger  $\mu_{S_1}$  will lead to an increase of  $k_r$ , which further result to a higher quantum yield. Table 3 shows that the  $\Delta E_{S_1-T_1}$  decreases in the following order: 1 > 1c > 1d > 1b > 1a (2 > 2d > 2c > 2b > 2a), with the smallest ones for 1a (0.3097 eV) and 2a (0.2218 eV). Thus, in comparison with the experimental structures of 1 and 2, the designed complexes 1a and 2a have a favorable ISC rate which would lead to a higher  $k_r$  for them. For  $\mu_{S_1}$ , the largest values were observed for 1a and 2a, implying their higher  $k_r$ . Obviously, the larger  $\mu_{S_1}$  and smaller  $\Delta E_{S_1-T_1}$  are needed for obtaining a large  $k_r$  value. Beside these factors, there are other factors also, that might play an important role for a higher quantum yield.

The higher-lying metal-centered (<sup>3</sup>MC d-d\*) (d represents the occupied molecular orbital which has great contributions from 5d orbitals of Ir and d\* represents the unoccupied molecular orbital which has some contributions from 5d orbitals of Ir) triplet excited states are considered to be one of the most important deactivation pathways of the phosphorescent emission from T<sub>1</sub> in transition-metal complexes.<sup>34,35</sup> In this regard, the selection of suitable stronger field ligands with sufficiently large ligand-centered (LC)  $\pi \rightarrow \pi^*$  transition energies and (or) <sup>3</sup>MLCT energies is necessary to raise the energy of d-d\* state. The lowest triplet metal-to-ligand charge transfer (<sup>3</sup>MLCT/ $\pi \rightarrow \pi^*$ ) excited state were obtained by performing an unrestricted triplet optimization starting from the optimized ground-state geometry. The electronic

configurations of  $^3\text{MC}$  d-d\* states were calculated using the previous studies,<sup>36,37</sup> in which optimization is starting with a distorted molecular geometry by largely elongating the metal-ligand bonds. The elongation of bond distances caused by the very weak chelating interaction between metal and ligands results in the larger nonradiative probability. This will decrease the quantum yield, which is controlled by the competition between the radiative ( $k_r$ ) and the nonradiative ( $k_{nr}$ ) rate. Theoretically, a larger separation between  $^3\text{MLCT}/\pi\rightarrow\pi^*$  and  $^3\text{MC}$  d-d\* states can bring a smaller  $k_{nr}$  and thus a higher phosphorescence quantum yield. By thermal activation, the  $^3\text{MLCT}/\pi\rightarrow\pi^*$  excited state can be rapidly converted, to a short-lived  $^3\text{MC}$  d-d\* state from which no photochemistry occurs,<sup>38,39</sup> and the conversion is often irreversible, due to the very fast nonradiative decay back to the ground state from the metal-centered state.<sup>35</sup> Thus, the energy gap between  $^3\text{MLCT}/\pi\rightarrow\pi^*$  and  $^3\text{MC}$  d-d\* states is the activation barrier for  $^3\text{MLCT}\rightarrow^3\text{MC}$  conversion.

A correlation between the N-substituted positions on the pyridine moiety in  $\text{N}^{\wedge}\text{N}$  ligands and  $^3\text{MLCT}/\pi\rightarrow\pi^*$  versus  $^3\text{MC}$  d-d state energy gap is showed in Fig. 5 with the normalized  $\text{S}_0$  levels.

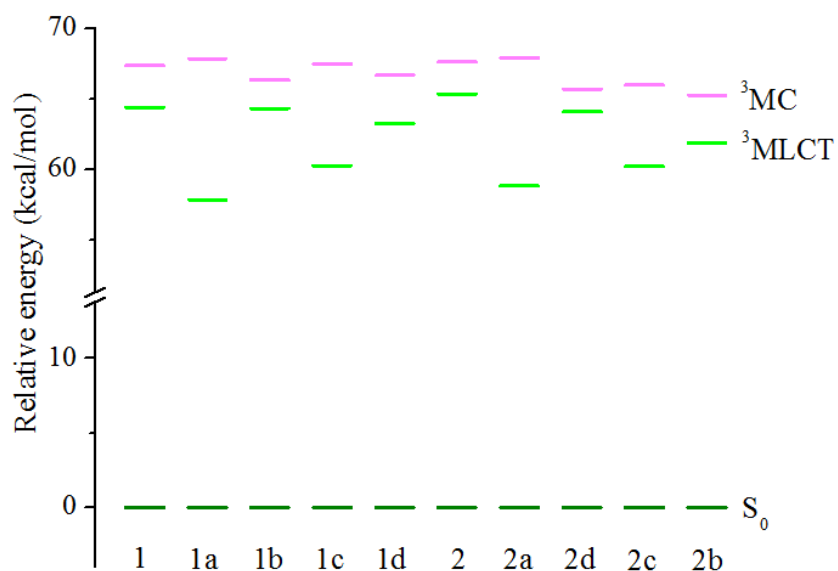


**Fig. 5** Energy level diagram of the studied complexes in  $^3\text{MLCT}/\pi\rightarrow\pi^*$  and  $^3\text{MC}$  d-d excited states respectively, along with the normalized  $\text{S}_0$  levels.

To evaluate the phosphorescence quantum yield, it is necessary to investigate the separation between  $^3\text{MLCT}/\pi\rightarrow\pi^*$  and  $^3\text{MC d-d}^*$  states, because a large separation between  $^3\text{MLCT}/\pi\rightarrow\pi^*$  and  $^3\text{MC d-d}^*$  states is believed to play a key role for maintaining the phosphorescence quantum yield. The energy gap  $^3\text{MLCT}/\pi\rightarrow\pi^*$  and  $^3\text{MC d-d}^*$  states of 2 is almost the same with that of 1 (Fig. 5) accounts for their similar nonradiative rate ( $k_{\text{nr}}$ ) of  $14\times 10^6$  and  $9\times 10^6 \text{ s}^{-1}$ ,<sup>19</sup> respectively. In addition, the results (Fig. 5) show a correlation between the N-substituted positions on the pyridine moiety in N<sup>^</sup>N ligands and  $^3\text{MLCT}/\pi\rightarrow\pi^*$  versus  $^3\text{MC d-d}^*$  state energy gap. We found the N substitution stabilizes the  $^3\text{MLCT}/\pi\rightarrow\pi^*$  states for 1a-1d and 2a-2d compared with 1 and 2. We also found that the energy level of  $^3\text{MLCT}/\pi\rightarrow\pi^*$  states for the assumed complexes 1a and 2a are significantly lower than other complexes. Meanwhile, the  $^3\text{MC d-d}^*$  states of 1a and 2a are lying at a relatively higher energy level among all these complexes. It can be seen clearly that the N substituent at the -a and -c position leads to a significantly larger energy gap between  $^3\text{MLCT}/\pi\rightarrow\pi^*$  and  $^3\text{MC d-d}^*$  states, which means the decrease of nonradiative pathway and a positive effect on improving the emission efficiency for these complexes.

To sum up, the lowest  $\Delta E_{\text{S}_1\text{-T}_1}$  and the higher  $\mu_{\text{S}_1}$  value for 1a and 2a, may account for a larger  $k_{\text{r}}$  according to equation (2). From the above discussion concerning  $^3\text{MC}$  and  $^3\text{MLCT}$  states, we can safely draw a conclusion that the complexes 1a and 2a are considered to have relatively higher  $\Phi$  due to the relatively larger  $k_{\text{r}}$  and smaller  $k_{\text{nr}}$ . Thus, 1a and 2a could be the potential blue-emitting material with high quantum efficiency. However, we should understand that besides the factors discussed above other factors may also affect radiative ( $k_{\text{r}}$ ) and nonradiative ( $k_{\text{nr}}$ ) rates.

## Conclusion

In this article, we reported the detail investigation of geometries structures, electronic structures, spectra and phosphorescence efficiency of two series of Ir(III) complexes. The phosphorescence wavelength, the photophysical properties and quantum yields of

these complexes are closely related to N substitution positions. Focused on the effect of the N substituted positions, a series of Ir(III) complexes on the basis of the structures of 1 and 2 have been designed by a systematic substitution of the “CH” group with the N atom at -a, -b, -c, and -d positions on the pyridine moiety in N<sup>^</sup>N ligands of 1 and 2, respectively. The calculated results showed that the Ir–N<sup>^</sup>N ligands bond lengths are significantly shortened for assumed complexes 1a-1d and 2a-2d as compared to those of experimentally found complexes 1 and 2, leading to more involvement of the N<sup>^</sup>N ligands in the frontier molecular orbitals and the excited states. Meanwhile, the systematic variation of N substitution in N<sup>^</sup>N ligands renders a decrease of HOMO-LUMO energy gap and stabilizes the energy levels of LUMOs more than HOMOs. The emissions spectra for the designed derivatives 1a, 1b, and 1d (2a, 2b, and 2d) are blue-shifted in comparison to complex 1 (2). In contrast, complex 1c (2c) show red shift compared with 1 (2). The calculated results reveal that the N substituent at the -a position can result in more contracted sphere structure relative to other complexes, and make the interaction between Ir and N<sup>^</sup>N moiety strengthened in 1a and 2a, which is the most important factor to increase the emission quantum yields. The largest energy gap between <sup>3</sup>MLCT/ $\pi$ - $\pi^*$  and <sup>3</sup>MC d-d\* states, lowest  $\Delta E_{S_1-T_1}$  and the higher  $\mu_{S_1}$  value increase the emission quantum yields of 1a and 2a than other complexes. It is also found that 1a and 2a are believed to be the potential blue emitters with high quantum efficiency.

## Acknowledgements

The authors are grateful to the financial aid from the National Natural Science Foundation of China (No. 21471022), the Program of Science and Technology Development Plan of Jilin Province of China (Grant No. 20140520090JH), the Science and Technology Research Project for the Twelfth Five-year Plan of Education Department of Jilin Province of China (Grant No. 201437), the Fund for Doctoral Scientific Research Startup of Changchun University of Science and Technology (Grant No. 40301855), and the Science and Technology Innovation Fund

of Changchun University of Science and Technology (Grant No. XJLJG-2014-12).

## References

- 1 R. Srivastava and L. R. Joshi, *Phys. Chem. Chem. Phys.*, 2014, **16**, 17284–17294.
- 2 J. L. Liao, Y. Chi, Y. D. Su, H. X. Huang, C. H. Chang, S. H. Liu, G. H. Lee and P. T. Chou, *J. Mater. Chem. C* 2014, **2**, 6269–6282.
- 3 D. Kourkoulos, C. Karakus, D. Hertel, R. Alle, S. Schmeding, J. Hummel, N. Risch, E. Holder and K. Meerholz, *Dalton Trans.*, 2013, **42**, 13612–13621.
- 4 S. L. Tao, S. L. Lai, C. A. Wu, T. W. Ng, M. Y. Chan, W. M. Zhao and X. H. Zhang, *Org. Electron.*, 2011, **12**, 2061–2064.
- 5 G. J. Zhou, C. L. Ho, W. Y. Wong, Q. Wang, D. G. Ma, L. X. Wang, Z. Y. Lin, T. B. Marder and A. Beeby, *Adv. Funct. Mater.*, 2008, **18**, 499–511.
- 6 M. A. Baldo, D. F. O'Brien, Y. You, A. Shoustikov, S. Sibley, M. E. Thompson, and S. R. Forrest, *Nature* 1998, **395**, 151–154.
- 7 W. Y. Wong and C. L. Ho, *J. Mater. Chem.*, 2009, **19**, 4457–4482.
- 8 C. Yang, S. L. Lai, S. R. L. F. Chan, K. H. Low, G. Cheng, K. T. Yeung, C. C. Kwok and C. M. Che, *Chem. Asian J.*, 2014, **9**, 3572–3585.
- 9 C. Adachi, M. A. Baldo, S. R. Forrest, S. Lamansky, M. E. Thompson and R. C. Kwong, *Appl. Phys. Lett.*, 2001, **78**, 1622–1624.
- 10 S. C. Yu, C. C. Kwok, W. K. Chan and C. M. Che, *Adv. Mater.*, 2003, **15**, 1643–1647.
- 11 C. M. Che, S. C. Chan, H. F. Xiang, M. C. W. Chan, Y. Liu and Y. Wang, *Chem. Commun.*, 2004, 1484–1485.
- 12 B. W. D'Andrade, R. J. Holmes, S. R. Forrest, *Adv. Mater.*, 2004, **16**, 624–628.
- 13 A. Tsuboyama, H. Iwawaki, M. Furugori, T. Mukaide, J. Kamatani, S. Igawa, T. Moriyama, S. Miura, T. Takiguchi and S. Okada, *J. Am. Chem. Soc.*, 2003, **125**, 12971–12979.
- 14 S. Lamansky, P. Djurovich, D. Murphy, F. Abdel-Razzaq, H. F. Lee, C. Adachi, P. E. Burrows, S. R. Forrest and M. E. Thompson, *J. Am. Chem. Soc.*, 2001, **123**,

- 4304–4312.
- 15 Y. Kawamura, S. Yanagida and S. R. Forrest, *J. Appl. Phys.*, 2002, **92**, 87–93.
- 16 C. Adachi, R. C. Kwong, P. Djurovich, V. Adamovich, M. A. Baldo, M. E. Thompson and S. R. Forrest, *Appl. Phys. Lett.*, 2001, **79**, 2082–2084.
- 17 R. J. Holmes, B. W. D’Andrade, S. R. Forrest, X. Ren, J. Li and M. E. Thompson, *Appl. Phys. Lett.*, 2003, **83**, 3818–3820.
- 18 S. J. Yeh, W. F. Wu, C. T. Chen, Y. H. Song, Y. Chi, M. H. Ho, S. F. Hsu and C. H. Chen, *Adv. Mater.*, 2005, **17**, 285–289.
- 19 Y. H. Song, Y. C. Chiu, Y. Chi, Y. M. Cheng, C. H. Lai, P. T. Chou, K. T. Wong, M. H. Tsai and C. C. Wu, *Chem. Eur. J.*, 2008, **14**, 5423–5434.
- 20 E. Runge and E. K. U. Gross, *Phys. Rev. Lett.*, 1984, **52**, 997–1000.
- 21 C. Adamo and V. Barone, *J. Chem. Phys.*, 1999, **110**, 6158–6170.
- 22 I. Avilov, P. Minoofar, J. Cornil, L. De Cola, *J. Am. Chem. Soc.*, 2007, **129**, 8247–8258.
- 23 A. D. Becke, *J. Chem. Phys.*, 1993, **98**, 5648–5652.
- 24 C. T. Lee, W. T. Yang and R. G. Parr, *Phys. Rev. B* 1988, **37**, 785–789.
- 25 P. J. Hay and W. R. Wadt, *J. Chem. Phys.*, 1985, **82**, 270–283.
- 26 T. Helgaker and P. Jørgensen, *J. Chem. Phys.*, 1991, **95**, 2595–2601.
- 27 E. Cancès, B. Mennucci and J. Tomasi, *J. Chem. Phys.*, 1997, **107**, 3032–3041.
- 28 M.J. Frisch, G.W. Trucks, H.B. Schlegel, G.E. Scuseria, M.A. Robb, J.R. Cheeseman, G. Scalmani, V. Barone, B. Mennucci, G.A. Petersson, H. Nakatsuji, M. Caricato, X. Li, H.P. Hratchian, A.F. Izmaylov, J. Bloino, G. Zheng, J.L. Sonnenberg, M. Hada, M. Ehara, K. Toyota, R. Fukuda, J. Hasegawa, M. Ishida, T. Nakajima, Y. Honda, O. Kitao, H. Nakai, T. Vreven, J.A. Montgomery Jr., J.E. Peralta, F. Ogliaro, M. Bearpark, J.J. Heyd, E. Brothers, K.N. Kudin, V.N. Staroverov, T. Keith, R. Kobayashi, J. Normand, K. Raghavachari, A. Rendell, J.C. Burant S.S. Iyengar, J. Tomasi, M. Cossi, N. Rega, J.M. Millam, M. Klene, J.E. Knox, J. B. Cross, V. Bakken, C. Adamo, J. Jaramillo, R. Gomperts, R.E. Stratmann, O. Yazyev, A.J. Austin, R. Cammi, C. Pomelli, J.W. Ochterski, R.L. Martin, K. Morokuma, V.G. Zakrzewski, G.A. Voth, P. Salvador, J.J.

- Dannenberg, S. Dapprich, A.D. Daniels, O. Farkas, J.B. Foresman, J.V. Ortiz, J. Cioslowski, D. J. Fox, Gaussian 09 (Revision B.01), Gaussian, Inc., Wallingford, CT, 2010.
- 29 N. M. O'Boyle, A. L. Tenderholt and K. M. Langner, *J. Comput. Chem.*, 2008, **29**, 839–845.
- 30 G. Tong and C. Che, *Chem. Eur. J.*, 2009, **15**, 7225–7237.
- 31 J. D. Chai and M. Head-Gordon, *Phys. Chem. Chem. Phys.*, 2008, **10**, 6615.
- 32 S. Sprouse, K. A. King, P. J. Spellane and R. J. Watts, *J. Am. Chem. Soc.*, 1984, **106**, 6647–6653.
- 33 M. G. Colombo, T. C. Brunold, T. Riedener, H. U. Güdel, M. Förtsch and H. B. Bürgi, *Inorg. Chem.*, 1994, **33**, 545–550.
- 34 J. Van Houten and R. J. Watts, *J. Am. Chem. Soc.*, 1976, **98**, 4853–4858.
- 35 T. Sajoto, I. Djurovich, A. B. Tamayo, J. Oxgaard, W. A. Goddard and M. E. Thompson, *J. Am. Chem. Soc.*, 2009, **131**, 9813–9822.
- 36 T. Bark and R. P. Thummel, *Inorg. Chem.*, 2005, **44**, 8733–8739.
- 37 M. Abrahamsson, M. J. Lundqvist, H. Wolpher, O. Johansson, L. Eriksson, J. Bergquist, T. Rasmussen, H. C. Becker, L. Hammarström and P. O. Norrby, *Inorg. Chem.*, 2008, **47**, 3540–3548.
- 38 K. Kalyanasundaram, *Academic Press: London*, 1992.
- 39 T. J. Meyer, *Pure Appl. Chem.*, 1986, **58**, 1193–1206